Surface charge density and evolution of domain structure in triglycine sulfate determined by electrostatic-force microscopy

J. W. Hong and K. H. Noh
Department of Physics and Condensed Matter Research Institute, Seoul National University, Seoul 151-742, Korea

Sang-il Park
PSIA Corporation, Seocho-dong 1600-3, Seoul 137-070, Korea

S. I. Kwun and Z. G. Khim
Department of Physics and Condensed Matter Research Institute, Seoul National University, Seoul 151-742, Korea
(Received 5 December 1997; revised manuscript received 23 February 1998)

A dynamic contact mode operation of electrostatic-force microscopy (EFM) with an ac modulation has been developed and used to investigate the domain strucutre and dynamics of a triglycine sulfate single crystal. Well-separated topographic and domain contrast images have been obtained by detecting the force instead of the force gradient in the dynamic contact mode operation of EFM. Surface charge density and the anisotropic domain wall thickness have been measured. The evolution of domains embedded in an oppositely polarized larger domain indicates the existence of a significant interaction between domains of the same polarity. [S0163-1829(98)05832-9]

I. INTRODUCTION

Ferroelectric materials have drawn considerable interest in recent years due to their wide application potential in, for example, laser optics and storage devices. The most promising application of ferroelectric materials seems to be a new nonvolatile semiconductor memory device. However, there are several problems such as electrical degradation and domain dynamics, which need to be solved or understood before the realization of a practical application of ferroelectric materials.

In order to facilitate the application of ferroelectric materials, it is, therefore, necessary to observe or control the formation of domain structures in ferroelectric materials.

Domain structures of ferroelectric materials have been studied by several methods such as surface etching, surface decoration, or electron microscopy, which are either destructive methods or require a special sample treatment. On the other hand, the recently developed scanning probe microscopy (SPM) proved to be very successful in taking images of the domain structure in ferroelectric materials.[1]

Advantages of SPM for the domain study are as follows: (i) it is a nondestructive method with no need of any special treatment, (ii) it allows a nanoscale visualization of the domain structure, and (iii) it allows control of the domain structure while taking images, i.e., domain reversal or movement.

However, the domain image by SPM so far is usually obtained by the noncontact mode operation,[1,2] which can detect basically the force gradient and, hence, the domain boundary image. Furthermore, the domain image obtained by this method is usually obscured by the superimposed topographic image of the surface. It was also reported that domain contrast obtained by a static contact mode of atomic force microscopy (AFM) reveals a topographic height difference[3] between differently polarized domains due to the interaction between tip and ferroelectric domain surface. A better detection method based on the piezoelectric vibration was used to differentiate the domain image from the topographic image of the ferroelectric material.[4,5] This method is better in distinguishing the domain contrast image, but still there remains some ambiguity regarding the piezoelectric deformation. These difficulties of SPM limit the reliable interpretation of the domain image.

In this work, we present domain contrast images of triglycine sulfate (TGS), which are completely separated from the topographic image. Triglycine sulfate, which has a Curie temperature of 49 °C, is one of the most widely studied ferroelectric materials.[6,7] TGS is known to show a spontaneous polarization along the *b* axis, i.e., domains of rod shape along the *b* axis with a lenticular cross section in the *a*-*c* plane possibly due to an anisotropy in the domain wall energy. Domain images of TGS in this work are obtained by the *dynamic contact mode operation of an electrostatic force microscope* (DC-EFM), which was originally designed to detect the distribution of the surface potential with the ac modulation technique.[8] In addition to the surface charge density due to the polarization, the evolution of domains, such as domain nucleation and growth at various temperatures, has been studied by the sequential measurement of the domain.

II. DETECTION METHOD

The sample studied in this work is a single crystal TGS grown by a slow evaporation from an aqueous solution. The thickness of the TGS crystal, cleaved in air, is approximately $\sim 400\ \mu$m.

An electrostatic force microscope (EFM) based on the electrostatic force modulation by applying an ac modulation voltage to the tip was built for the study of the potential as well as the charge-density distribution on the sample surface.

In the *dynamic* noncontact mode of EFM, which is operated in the presence of an attractive force between tip and

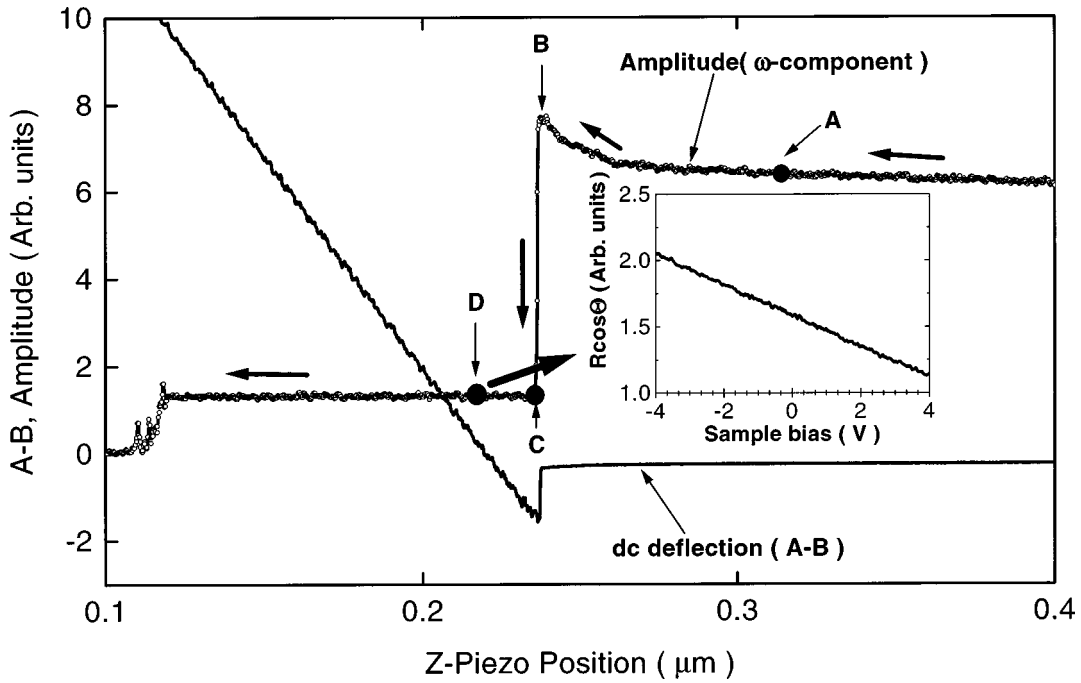

FIG. 1. Vibration amplitude (ω component) and dc deflection signal for a cantilever with a force constant k=1.9 N/m. The applied ac voltage amplitude and frequency are 3 V and 40 kHz. The origin for the tip-sample distance is arbitrary. Below point *C*, where the tip is making contact with the sample surface, there still remains a finite vibration amplitude. The actual measurement for the domain contrast and topographic image is made near point *D*. In the inset, $R\cos\theta$ is the in-phase component of the lock-in output at frequency ω.

sample, the resonance frequency of a cantilever is affected by the force gradient on the sample surface. The vibration amplitude of the cantilever is hence affected by the variation of the force due to changes in electrical properties such as the domain boundary in ferroelectric materials as well as due to the change in the topography. This is how one can detect a domain boundary in ferroelectric materials[9] by means of the noncontact EFM. Therefore, in the noncontact dynamic mode, the effect of a force gradient due to a topographic change is mixed with that due to a domain boundary making it difficult to differentiate between them.[1]

In the static contact mode of the EFM, the force on the tip consists of an atomic force and an electrostatic force,

$$F = F_a + F_e . \tag{1}$$

The static deflection of the tip is mainly influenced by the repulsive atomic force in the contact mode. If the static atomic force is employed as the feedback signal, the topography of a sample can be obtained with a high lateral resolution while the tip-surface distance will be virtually fixed by the strong atomic repulsive force.

If it is possible to operate an EFM in a dynamic contact mode, the topography of the sample can be obtained just as in the contact mode operation, while the electrical property of the surface can be studied by detecting the electrostatic force in a similar way to that of the noncontact operation. Thus the electrostatic effect in the surface can be separated from the topographic effect in the dynamic contact mode. In addition, the spatial resolution in the contact mode operation can be improved because of a short distance between tip and sample compared to that in a noncontact mode operation.

Figure 1 shows the vibration amplitude (ω component) and dc deflection curves of a cantilever with a force constant k = 1.9 N/m. In the actual operation of the EFM with a modulation bias $V_{ac}\cos\omega t$, the vibration amplitude of the tip is initially growing in the noncontact region (*A*) and then is reduced drastically in the tapping region (*B*) as the tip approaches the sample surface as shown in Fig. 1.[10] At point *C*, the dc deflection signal of the cantilever indicates that the tip is making contact with the sample surface. Further decrease in the distance will bend the cantilever resulting in a dc deflection signal that is proportional to the decrease in the distance as shown in the figure. Unexpectedly, however, there remains a finite vibration amplitude even in the contact region (*D*). Of course for a soft material, a small vibration amplitude in the contact region was already reported and is possible through the mechanical indentation of the soft surface, which allows measurments for the elasticity variation of a sample.[11] But, sustained vibration of the cantilever on a hard surface, like ferroelectrics, even in a contact state is a surprising result that allows a new dynamic contact mode operation of EFM. We observed this *sustained vibration* in the contact state for various hard surfaces, some of which are not ferroelectric materials. The inset of Fig. 1 shows a plot of the vibration amplitude versus dc bias voltage at frequency ω obtained for a nonferroelectric sample (Si wafer). The linear dependence of the vibration amplitude on the bias is unequivocal evidence indicating that the sustained vibration of the cantilever is not an artifact but a real effect related to the electrical property of the sample surface.

The sustained vibration of the tip in the contact state opens the possibility of operating an EFM in a dynamic contact mode. Actually, we have succeeded in taking the topographic image and surface potential of a semiconducting test sample simultaneously by the dynamic contact mode operation of the EFM (contact mode operation of the EFM with

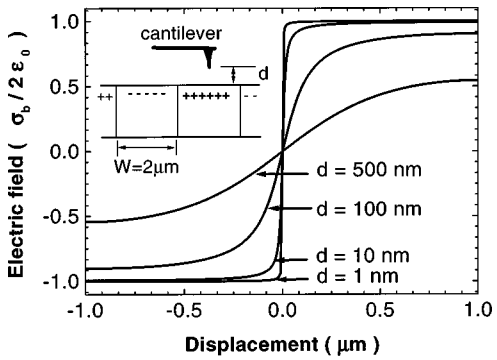

FIG. 2. Calculated electric field for strips with alternating surface charge density $\pm\sigma_b$ as a function of the height from the surface. Here, the shape of the domain is assumed to be fingerlike with a width $w=2$ μm. For d smaller than several nm, the electric field can be safely regarded as an uniform electric field $E_s=\sigma_b/2\epsilon_o$.

modulation), which shows a better resolution than the noncontact mode EFM. It is required to use an insulated tip to prevent any unintentional charging during the contact mode operation. The probe tip used in this work is a heavily doped Si (doping level is 10^{19}–$10^{20}/\mathrm{cm}^3$) with a spring constant k = 1.9 N/m and a typical tip radius $R=40$ nm. It seems that the surface of the tip is covered with a SiO_2 oxide layer, thus preventing current flow between the tip and sample.

Now, for the quantitative analysis and detection mechanism of the domain in a ferroelectric material, consider a surface with a polarization charge density. In the presence of a bound surface charge density σ_b as in the case of the ferroelectric domain, the electrostatic force F_e on a tip is given as a sum of a capacitive force and a Coulombic force between the tip and sample surface.[12] Since the tip-sample distance is short in a contact mode operation, one can approximate the effect of bound surface charge density by a uniform electric field. Figure 2 shows the calculated electric field above oppositely polarized domains as function of the height from the domain surface. Here the shape of domain is assumed to be fingerlike with a domain width of 2 μm, which is a typical value for TGS. The electric field at a distance d less than a few nm can be regarded as a constant field $E_s=\sigma_b/2\epsilon_o$, but for d larger than 10 nm, a wide electric field variation appears near the domain boundary. Therefore, in a noncontact EFM operation, the variation in the electrostatic force gradient can shift a resonance frequency of the cantilever, perturbing the topography measurement. However, in the operation of the DC-EFM, the tip-sample distance is of the order of 1 nm controlled only by an atomic repulsive force instead of a force gradient. Thus topography is well separated from the electrical property of the surface.

Using the constant electric field approximation, Coulombic force can be expressed simply as $E_s q_t$, where $E_s=\sigma_b/2\epsilon_o$ is the electric field due to a constant bound surface charge density $\sigma_b=\mathbf{P}\cdot\mathbf{n}$ and q_t is the charge induced at the tip by the applied voltage V, $q_t=CV$. The electrostatic force is, therefore, given as

$$F_e=\frac{1}{2}\frac{\partial C}{\partial z}V^2+E_s q_t=\frac{1}{2}\frac{\partial C}{\partial z}V^2+\frac{\sigma_b C V}{2\epsilon_o}. \tag{2}$$

Here, the applied bias between the tip and sample can have both dc and ac modulation components $V=V_{\mathrm{dc}}+V_{\mathrm{ac}}\cos\omega t$. Substituting V in Eq. (2), one has

$$\begin{aligned}F_e&=\frac{1}{2}\frac{\partial C}{\partial z}(V_{\mathrm{dc}}+V_{\mathrm{ac}}\cos\omega t)^2+\frac{\sigma_b C}{2\epsilon_o}(V_{\mathrm{dc}}+V_{\mathrm{ac}}\cos\omega t)\\&=\frac{1}{2}\frac{\partial C}{\partial z}\left(V_{\mathrm{dc}}^2+\frac{V_{\mathrm{ac}}^2}{2}\right)+\frac{\sigma_b C V_{\mathrm{dc}}}{2\epsilon_o}+\left(\frac{\partial C}{\partial z}V_{\mathrm{dc}}+\frac{\sigma_b C}{2\epsilon_o}\right)\\&\quad\times V_{\mathrm{ac}}\cos\omega t+\frac{1}{4}\frac{\partial C}{\partial z}V_{\mathrm{ac}}^2\cos 2\omega t.\end{aligned} \tag{3}$$

Thus the mechanical deflection of the cantilever due to the electrostatic force will have dc, ω, and 2ω components. The dc and 2ω components contain the topographic information of the sample via $\partial C/\partial z$, while the ω component contains the information on the surface charge density σ_b of the sample.

Therefore one can use the dc components of F, which includes the dominant strong repulsive atomic force F_a in addition to the dc part of the electrostatic force as the control feedback signal to maintain a constant height in the contact mode operation of EFM. Actually the topographic image in this work was obtained from this signal.

Since the amplitude of the ω component from the lock-in amplifier depends both on V_{dc} and on the surface polarization charge density σ_b, measurement of the ω component of the cantilever oscillation leads to the detection of the bound surface charge density or the domain image. Thus for a ferroelectric material with an 180° domain such as TGS, one can expect two level surface charge densities corresponding to either a positively or negatively polarized surface.

The DC-EFM, explained here, is different from the piezoreponse method introduced by Franke *et al.*,[13] in that the piezoresponse method is detecting the thickness variation of a sample, covered with an adsorbate layer, due to the piezoelectric effect, while the DC-EFM is detecting the electric force variation caused by the surface charge density. In the piezoresponse model, the protrusion or contraction of a ferroelectric sample is attributed to the piezoelectric effect of the sample. However, there remain some questions as to the piezoresponse interpretation by the piezoelectric effect. First, we could not observe any protrusion or contraction on differently polarized regions within the vertical resolution limit of 0.1 nm in our measurement for a freshly cleaved TGS sample. More importantly, the expected domain thickness variation in the piezoresponse model, $\delta t=\int_R^d d_{22}E(t)dt$, is less than $\sim$0.01 nm at most for a typical sample of thickness 1 mm, piezoresponse coefficient $d_{22}=20\times10^{-12}$ m/V,[14] and a polarization field at the tip surface $E(R)=10^7$ V/m. Thus, it will be very difficult to detect this thickness variation. Furthermore, the piezoelectricity d_{22} of TGS shows a strongly increasing trend as the temperature approaches T_c. Then the piezoresponse signal should show a more pronounced domain image as the temperature increase toward T_c. However, the actual measurement shows a rather diminishing domain contrast as the temperature increases. This evidence indicates that the detection mechanism of the domain contrast is not due to the piezoresponse effect but due to the electric-field effect of the ferroelectric surface.

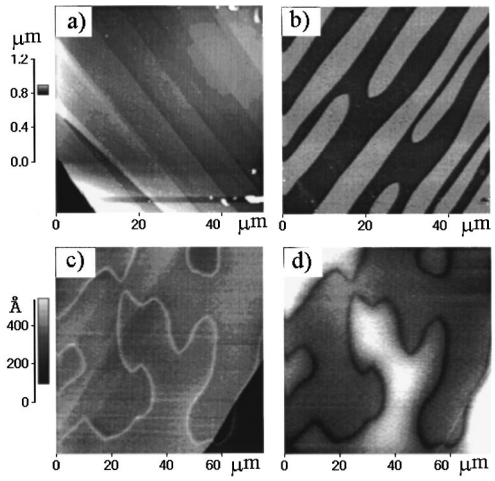

FIG. 3. Comparison between images obtained by the DC-EFM and noncontact EFM. Images obtained by DC-EFM do not show any correlation between topography (a) and domain contrast (b) image. However, images obtained by the noncontact EFM show a significant coupling between topography (c) and charge (d) image.

Figure 3 shows the difference in the topographic and domain contrast images that are obtained by DC-EFM and noncontact EFM methods. Both topographic and domain contrast image are obtained simultaneously at a different location for each method. Topography (a) and domain image (b) are well separated in DC-EFM. No protrusion or contraction related to the domain is observable in the topographic image. The charge-density image shows distinctly two levels of dark and bright regions corresponding to the positively and negatively polarized domain, respectively. However, the topography [Fig. 3(c)] and surface charge image [Fig. 3(d)] obtained by the noncontact EFM method overlap. In the topographic image, there appears a pronounced domain boundary image due to a strong electrostatic force gradient at the boundary. In addition, the topographic image shows a somewhat poorer lateral resolution than the one obtained by the DC-EFM. The domain image [Fig. 3(d)] shows a gray scale that changes smoothly from the center of the domain to the boundary. This is not because of the variation in the polarization but because of the variation in the electric field at the boundary in the noncontact mode of the EFM as explained in Fig. 2. From this measurement, we are convinced that the DC-EFM is detecting the surface charge density rather than the piezoresponse of the sample.

III. RESULTS AND DISCUSSIONS

Domain contrast and topographic images of TGS are simultaneously measured by the DC-EFM with the dc bias V_{dc} set equal to zero. The estimated distance between tip and sample is ~ 1 nm obtained from the amplitude of the tip vibration.

Figure 4 shows well-separated topographic and domain contrast images of the TGS(010) surface obtained simultaneously with $V_{dc}=0$, $V_{ac}=5$ V, and $f = 40$ kHz. The enlarged topographic image (not shown here) of the TGS surface shows cleavage steps of ~ 12 Å which is very close to the lattice unit $b=12.69$ Å.[15] The domain image or domain boundary does not appear in the topographic image in this

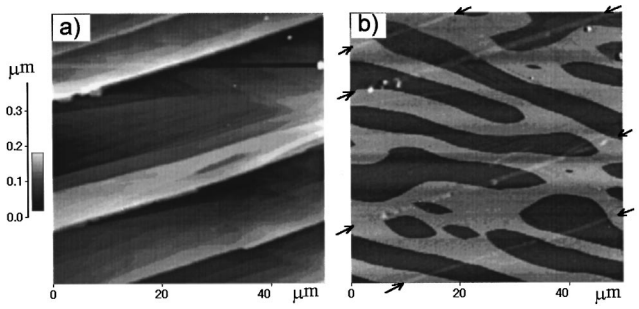

FIG. 4. Topographic image (a) and domain contrast (b) of a cleaved TGS obtained simultaneously. Careful inspection of the domain image shows a faint shadowy topographic image along the cleaved step on the surface, as indicated by arrows. But there appears to be no structure related to the domain in the topographic image.

work as it does in previous reports,[1,2,16] where a piezoelectric effect in the polarized sample is suspected to cause such a topographic height difference depending on the polarization. Domain contrast shows in general only two level contrast in good agreement with our expectation based on Eq. (3).

Careful inspection of the domain contrast, however, reveals a faint shadowy topographic image along cleaved steps on the surface as indicated by arrows in Fig. 4(b). This appearance of the topographic shadow in the domain contrast can be understood as a result of a severe local variation of capacitance C at the step edge on the cleaved surface. Constant height operation of the DC-EFM, which is equivalent to a constant capacitance operation, fails momentarily while scanning over such a step edge. The change of the capacitance at such a step from C to C' will produce a change in the ω component, $\sigma_b C'/2\epsilon_o$, as if there is a change in the surface charge density, $\sigma_b'=\sigma_b C'/C$, on a smooth surface where one can maintain a constant height operation of the DC-EFM. The appearance of shadow topographic images observed at step edges is evidence indicating the correctness of our analysis.

Domain structure, however, is not affected by the cleavage step or slope on the cleaved surface. There is no protruded or submerged step related to the domain wall in the topographic image as there is in previous reports.[1,17,18] The explanation by a protrusion due to the piezoelectric deformation was also questioned by Takata[19] who proposed an alternative cause, electrochemical activity. Of course we could not detect any hysteretic behavior in the domain image depending on the forward and backward scan direction.[1,20]

The general appearance of the domain structure reveals a fingerlike or an elongated lenticular shape similar to that of earlier reports.[2,16] The elongated lenticular shape is attributed to the anisotropic domain wall energy in TGS. If there is an anisotropy in the domain energy as is suspected in the case of TGS, one can expect a variation of the domain wall width depending on the direction in the a-c plane. Figure 5 shows a small positively polarized domain of roughly elliptic shape with a semimajor axis $a=1.17$ μm and semiminor axis $b=0.53$ μm. The domain shape at the end of the major axis shows a rather sharp corner with its angle ranging from 60° to 120°, thus lenticular is more adequate than elliptic in describing the shape of the TGS domain.

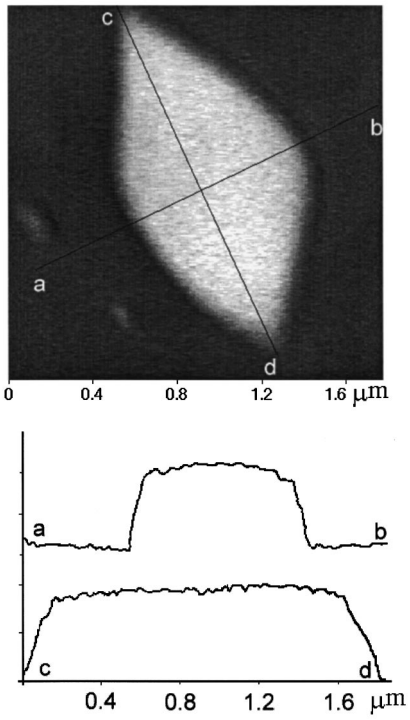

FIG. 5. Negatively polarized domain of a lenticular shape. Domain wall thickness estimated along the semimajor and semiminor axis are ~110 nm and ~60 nm at 20 °C.

Typical domain wall thicknesses measured at 20 °C for this particular domain are ~110 nm and ~60 nm along the semimajor and semiminor axes, respectively. To avoid any artifact caused by the scan direction, we measured the wall thickness of several domains at different angles. Of course there is some variation in the thickness of the domain wall depending on the sample. In one instance, we observed a sizable variation of the domain wall thickness ranging from 30 to 80 nm in the semiminor direction. However, the wall width ratio along the major axis and along the minor axis remains close to 1.8. Of course, the typical value of the domain wall reported in this work is an upper limit because of the finite tip radius of ~40 nm. This value is much larger than reported values of 10 nm (Ref. 2) and 8 nm (Ref. 16) but much smaller than 600–800 nm.[17]

An attempt is made to measure the bound surface charge density $\sigma_b = \mathbf{P}\cdot\mathbf{n}$ induced by the polarization. Since the ω component in F_e [Eq. (3)] is proportional to $(\partial C/\partial z V_{\rm dc} + \sigma_b C/2\epsilon_o)$, one can, in principle, estimate σ_b from the amplitude of the ω component. With $V_{\rm dc}\neq 0$, a difficulty in estimating σ_b arises due to the asymmetric dependence of $|F_\omega|$ on the surface charge density as was pointed out by Ogahmi *et al.*[17] Even with $V_{\rm dc}=0$, one needs to know the capacitance between tip and sample to estimate the bound charge density. Furthermore a spurious bias induced by defects or by local charges on the sample can easily complicate the analysis for the charge density. Instead of measuring the amplitude of $|F_\omega|$, we can adjust the dc tip bias $V_{\rm dc}$ until the amplitude of $|F_\omega|$ vanishes. In this nulling method, the surface charge density is related to the null bias $V_{{\rm dc},n}$ as $\sigma_b = -2\epsilon_o V_{{\rm dc},n}(\partial C/\partial z)/C$. This nulling method has several advantages over the amplitude measurement; for example, the nulling method can overcome the ambiguity related to the asymmetric behavior of $|F_\omega|$ or the necessity for the absolute value of C and $\partial C/\partial z$. Since the EFM is operated in a contact mode with the tip to sample distance as small as 1 nm in this work, the capacitance between tip and sample can be treated as a parallel plate capacitor with the resulting $(\partial C/\partial z)/C \cong 1/d$, where d is the distance between tip and sample. The measured difference between the nulling bias $\delta V = V^+_{dc,n} - V^-_{dc,n}$ corresponding to the positively and negatively polarized TGS domains at 20 °C was 3.1 V with a measurement uncertainty less than 0.1 V. A rough estimate for the distance d between tip and sample was made from the force distance curve, assuming the vibration amplitude to be equal to the average distance d in the contact mode operation. By comparing the magnitude of the vibration amplitude signal (90–110 mV) of the cantilever with that of the deflection signal (1.9 V) of a very large scale integrated height standard of 18 nm, we obtained $d = 1 \pm 0.1$ nm. The uncertainty was mainly due to the fluctuation of the vibration amplitude signal. The resulting surface charge density of TGS at 20 °C obtained by this method is $\sigma_b = 2.7 \pm 0.3$ μC/cm^2. This is in a good agreement with the reported value of 2.8 μC/cm^2,[21] considering our crude estimate on the gap between tip and sample. To improve the accuracy in the estimate of σ_b , it is required to reduce the uncertainty in the gap distance between tip and sample. Also note that the effective electrostatic distance between tip and sample could be different from the measured value due to the presence of an insulating layer on the tip surface.[22] Therefore the good agreement in the σ_b value can be regarded as an alternative method for the estimate of the effective distance between tip and sample.

Since a well-defined domain contrast can be obtained from our DC-EFM, we studied the evolution of the ferroelectric domain structure in TGS. An earlier attempt by Luthi *et al.*[23] for the domain dynamics of TGS employed a noncontact mode operation, which can only take images of domain boundaries. Besides, they applied a nonzero $V_{\rm dc}$ to the probing tip during scanning, which can alter the shape of domains under study. Frictional force microscope[24] was also used to study the domain change in TGS. To investigate the evolution of the domain in this work, we brought the TGS sample into a nonequilibrium state by heating up the sample above Curie temperature and then subsequently cooling down to room temperature, 20 °C. Certainly above T_c , the domain contrast disappeared. In less than 30 sec after cooling down, the sample temperature reached an equilibrium temperature in air. For this reason, we began to acquire images of the TGS domain 30 sec after cooling to room temperature. With a scanning speed of 1 Hz, it is actually impossible to take a domain image earlier than this due to a rapid domain evolution at the earlier cool-down period. We took domain images every 4 min up to 1 h. Figure 4 shows TGS domain images taken sequentially up to 1 h. Inside of the fingerlike domain with an average domain width of ~2 μm, there are many oppositely polarized lenticular-shape domains accompanied by several smaller satellite domains of the same polarization. These isolated domains embedded in the oppositely polarized fingerlike domain gradually diminish. However, the fingerlike domain does not change its size or shape up to 1 h, the duration of our obser-

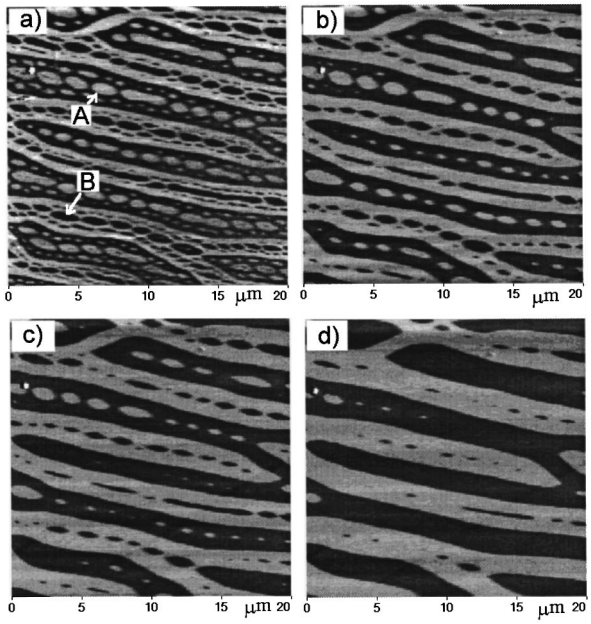

FIG. 6. A sequence of domain contrasts of TGS taken at (a) 30 sec, (b) 4 min, (c) 20 min, and (d) 52 min after cooling to room temperature from above T_c. Small isolated domains gradually diminish, while finger-shaped domains do not change their shape and size up to 1 h.

vation. The area of the positively polarized domain observed with $V_{dc}=0$ remained equal to that of negatively polarized domain during the domain evolution, indicating no preference in domain orientation in the scale of 20×20 μm.

The size of two particular isolated domains, one positively and the other negatively polarized, indicated by arrows in Fig. 6(a), show an increasing trend until the surrounding satellite domains disappear. Once satellite domains disappear, then the size of the isolated domain begins to decrease. Figure 7 shows the time dependent domain size of two isolated and oppositely polarized domains, indicated by arrows as shown in Fig. 6(a). Except for the initial increasing trend, the isolated domain shows almost a linear decreasing behavior while the width of a fingerlike domain remains virtually constant at 2.4 ± 0.04 μm. Our observation indicates that the

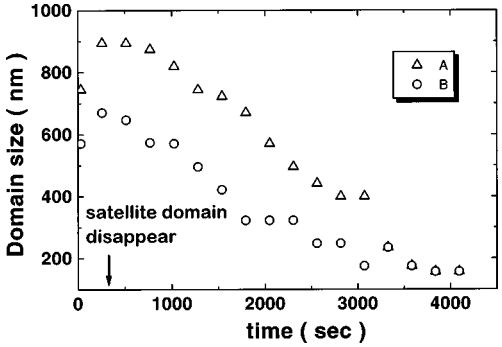

FIG. 7. The change in the diameter (along the minor axis) of isolated domains in TGS that was brought into a nonequilibrium state: positively polarized domain A ($\triangle$) and negatively polarized domain B ($\bigcirc$) indicated by arrows in Fig. 6. The diameter increases initially until the surrounding smaller satellite domain disappears, then decreases almost linearly in time.

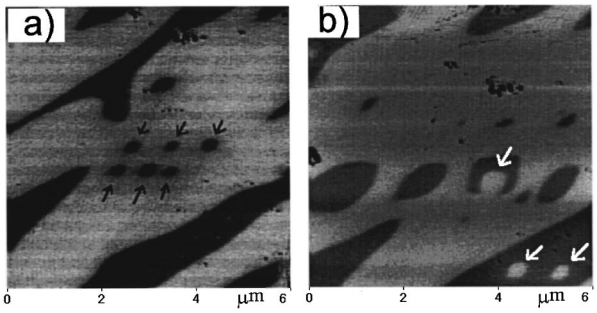

FIG. 8. Growth of new positively polarized domains indicated by arrows in (a) under a tip bias of $V_{dc}=-10$ V. Circular initial shape of the new domain relaxes to a lenticulat shape. White dots (negatively polarized domain) are written under a tip bias $V_{dc}=10$ V.

shape of the larger-size domain, in this case the fingerlike domain, is fixed with a much shorter relaxation time while the evolution of a small domain embedded in a larger domain is determined by a much longer relaxation time of the order of 1 h in the case of TGS at 20 °C. If there is no interaction between neighboring domains of the same polarization, the size of small domains surrounded by oppositely polarized domains should show a monotonically decreasing trend only. Therefore, the complex variation of the size observed in small domains embedded in oppositely polarized domains is interpreted as an implication of the interaction between adjacent domains of the same polarization.

Finally, a polarization reversal under a tip bias has been observed. Domain reversal depends on the magnitude and duration of the applied tip bias V_{dc}. Evolution of the newly created domain, such as the change of domain size or shape, seems to depend on the surface condition. For example, on a freshly cleaved surface of TGS, it was rather difficult to observe the domain reversal due to a rapid relaxation of the reversed polarization to its original polarization. However, on a much degraded surface, the evolution of the reversed domain was slow enough to take the domain image. We speculate that the degraded surface layer is producing a pinning effect by lowering domain energy. Dark spots indicated by arrows in Fig. 8(a) are written on a degraded surface (surface exposed to air for more than a week) under a tip bias $V_{dc}=-10$ V. The shape change from an initially circular to lenticular shape is due to the evolution of domains. From this we confirmed that the polarity of the dark contrast corresponds to the positively polarized domain. White dots in Fig. 8(b) are written under $V_{dc}=10$ V. The threshold bias for a domain reversal in this work is approximately 7 V. The electric field near the tip under a bias of 7 V is about 1.7×10^8 V/m, which is much stronger than the reported coercive field,[14] which is on the order of 10^4–10^5 V/m.

IV. CONCLUSION

With a modified analysis for the electrostatic force between tip and charged surface, the surface charge density and dynamics of ferroelectric domains in a TGS single crystal were studied by the dynamic contact mode operation of an ac modulated EFM. In this method, the cantilever vibration persisted even in the contact situation, thus allowing a simulta-

neous measurement of topographic and domain contrast images. Unlike previous authors, we did not observe any morphology change due to the domain formation in TGS.

TGS exhibits 180° domains of fingerlike shape with oppositely polarized domains of a lenticular shape embedded inside. The bound surface charge density obtained in this work is $\sigma_b = 2.7\ \mu C/cm^2$ at 20 °C, which is very close to the reported value of 2.8 $\mu C/cm^2$. The upper limit of domain wall thickness is ~110 nm and ~60 nm along the semimajor and semiminor axes with the anisotropy ratio 1.8.

The size variation of domains embedded in an oppositely polarized domain indicates that there is significant interaction between domains of the same polarity. The relaxation of smaller domains shows an almost linear time dependence. Furthermore, the degraded surface layer seems to have a pinning effect on the evolution of the domain by lowering, for example, the surface energy of the domain. The threshold bias for a domain reversal on a TGS single crystal in this work is about 7 V. Of course, more detailed investigation, such as temperature dependence or dependence on the distance between domains, is required to elucidate the dynamics of domains in ferroelectrics.

ACKNOWLEDGMENTS

This work was supported in part by the Nano-Structure Technology Project and also by the Ministry of Education in Korea under Grant No. BSRI-97-2416.

[1] R. Luthi, H. Haefke, K.-P. Meyer, E. Meyer, L. Howald, and H.-J. Guntherrodt, J. Appl. Phys. **74**, 7461 (1993).
[2] M. K. Bae, T. Horiuchi, K. Hara, Y. Ishibashi, and K. Matsushige, Jpn. J. Appl. Phys., Part 1 **33**, 1390 (1994).
[3] O. Kolosov, A. Gruverman, Jun Hatano, K. Takahashi, and H. Tokumoto, Phys. Rev. Lett. **74**, 4309 (1995).
[4] A. Gruverman, O. Auciello, and H. Tokumoto, J. Vac. Sci. Technol. B **14(2)**, 602 (1996).
[5] A. Gruverman, O. Auciello, R. Ramesh, and H. Tokumoto, Nanotechnology **8**, A38 (1997).
[6] B. T. Mattias, C. E. Miller, and J. R. Remeika, Phys. Rev. **104**, 849 (1956).
[7] N. Nakatani, Jpn. J. Appl. Phys. **12**, 1723 (1973).
[8] Detailed measurement technique will be published elsewhere.
[9] H. Bluhm, A. Wadas, R. Wiesendanger, K. P. Meyer, and L. Szczesniak, Phys. Rev. B **55**, 4 (1997).
[10] J. W. Hong, Z. G. Khim, A. S. Hou, and Sang-il Park, Appl. Phys. Lett. **69**, 2831 (1996).
[11] P. Maivald, H. J. Butt, S. A. C. Gould, C. B. Prater, B. Drake, J. A. Gurley, V. B. Elings, and P. K. Hansma, Nanotechnology **2**, 103 (1991).
[12] B. D. Terris, J. E. Stern, D. Rugar, and H. J. Mamin, Phys. Rev. Lett. **63**, 2669 (1989).
[13] K. Franke, J. Besold, W. Haessler, and C. Seegebarth, Surf. Sci. Lett. **302**, L283 (1994); K. Franke, Ferroelectr. Lett. Sect. **19**, 25 (1995); K. Franke, H. Huelz, and S. Seifert, *ibid.* **23**, 1 (1997).
[14] Toshio Mitsui, *et al.* in *Numerical Data and Functional Relationships in Science and Technology*, edited by K.-H. Hellwege and A. M. Hellwege, Landolt-Börnstein, New Series, Group III, Vol. **3** (Springer-Verlag, Berlin, 1969), pp. 495–496.
[15] H. Bluhm and R. Wiesendanger, J. Vac. Sci. Technol. B **14**, 1180 (1996).
[16] L. M. Eng, M. Friedrich, J. Fousek, and P. Gunter, J. Vac. Sci. Technol. B **14**, 1191 (1996).
[17] J. Ohgami, Y. Sugawara, S. Morita, E. Nakamura, and T. Ozaki, Jpn. J. Appl. Phys., Part 1 **35**, 2734 (1996).
[18] A. Gruverman, O. Kolosov, Jun Hatano, K. Takahashi, and H. Tokumoto, J. Vac. Sci. Technol. B **13**, 1095 (1995).
[19] K. Takata, J. Vac. Sci. Technol. B **14**, 3393 (1996).
[20] M. K. Bae, K. Hara, H. Okabe, S. Kai, and Y. Ishibashi, J. Phys. Soc. Jpn. **65**, 2401 (1996).
[21] M. E. Lines and A. M. Glass, *Principle and Applications of Ferroelectrics and Related Materials* (Clarendon, New York, 1982), p. 629.
[22] The effective electrostatic distance will be different from the measured tip sample distance due to the presence of an insulating layer on the tip surface. Thus the measured distance from the force distance curve should be regarded as a lower limit of the effective distance. This was pointed out by the referee.
[23] R. Luthi, H. Haefke, W. Gutmannsbauer, E. Meyer, L. Howald, and H.-J. Guntherrodt, J. Vac. Sci. Technol. B **12**, 2451 (1994).
[24] A. Correia, J. Massanell, N. Garcia, A. P. Levanyuk, A. Zlatkin, and J. Przeslawski, Appl. Phys. Lett. **68**, 2796 (1996).